

Quantum-classical correspondence in the $O(^3P)+HCl$ and $Cl(^2P)+OH$ reactions for total angular momentum $J=0$

Yongjing Lin and B. Ramachandran^{a)}

Chemistry, College of Engineering and Science, Louisiana Tech University, Ruston, Louisiana 71272

Katsuyuki Nobusada

Division of Chemistry, Graduate School of Science, Hokkaido University, Sapporo, Hokkaido 060-0810, Japan

Hiroki Nakamura

Department of Theoretical Studies, Institute for Molecular Science, Myodaiji, Okazaki 444-8585, Japan

(Received 26 June 2000; accepted 3 November 2000)

A method for carrying out quasiclassical trajectory (QCT) calculations of $A+BC(v,j)$ reactive collisions for the special case of the total angular momentum $J=0$ is described. Since quantum reactive scattering calculations involving heavier atoms are not straightforward for the $J>0$ case, this method is useful to establish the extent to which classical mechanics is applicable to a particular reaction. The method is tested by comparing the results of trajectory calculations for the $J=0$ case with analogous quantum-mechanical (QM) calculations for the $O(^3P)+HCl$ reaction and the reverse reaction $Cl(^2P)+OH$. The S4 potential surface, which is based on MRCI+Q/cc-pVTZ energies scaled by the scaled external correlation method [B. Ramachandran *et al.*, *J. Chem. Phys.* **111**, 3862 (1999)], is used for these calculations. The QCT and QM cumulative reaction probabilities are found to be in good agreement, especially for the $Cl+OH$ reaction. The agreement between the two types of state-resolved reaction probabilities is less striking but improves considerably as the initial diatomic rotational quantum number j increases. A comparison is also made between the exact and J -shifted QCT thermal rate coefficients. These are found to be in excellent agreement, which is in keeping with similar agreement observed in the case of the quantum-mechanical exact and J -shifted thermal rate coefficients. © 2001 American Institute of Physics. [DOI: 10.1063/1.1335657]

I. INTRODUCTION

There is a fundamental difference in the way the total angular momentum \mathbf{J} (boldface indicates a vector quantity here and throughout) is treated in the quantum-mechanical (QM) and quasiclassical trajectory (QCT) formulations of the atom–molecule reactive collision problem. In quantum mechanics, since the Hamiltonian is block diagonal in the total angular momentum quantum number J , it is natural to formulate and solve the scattering problem for each fixed value of J .¹ In order to obtain the integral reaction cross section, one performs calculations for all values of J for which the reaction probabilities are non-negligible. On the other hand, in the QCT approach, it has been customary to allow the (unquantized) total angular momentum to vary in a random fashion from trajectory to trajectory so that the initial state-selected integral reaction cross section is directly obtained by propagating a sufficiently large ensemble of trajectories.² This means that direct comparisons of quantum and classical behavior for reactive atom–molecule collisions are most easily done for those few cases where a fully converged quantum reaction cross section can be calculated. Several such comparisons exist (for example, see Refs. 3–7), and these generally support the notion that classical mechan-

ics provides rather accurate descriptions of atom–diatomic molecule ($A+BC$) reactions at relatively high energies.

Methods for choosing trajectory initial conditions such that J lies within a specified range $0 \leq J \leq J_{\max}$ ($J_{\max} > 0$) have been described by Truhlar and co-workers.⁸ In these calculations, the impact parameter b is constrained to lie between two limits. This restricts the magnitude, but not the direction, of the orbital angular momentum vector \mathbf{l} , which now is obtained as a random value between a minimum and maximum. However, since $\mathbf{J} = \mathbf{j}_r + \mathbf{l}$ (i.e., by vector addition) where \mathbf{j}_r is the rotational angular momentum of the diatomic molecule, it is still possible to get trajectories with $J > J_{\max}$, which are rejected from the ensemble. Comparisons of QCT partial cross sections calculated in this manner to analogous QM quantities for the $H+H_2$,⁸ $D+H_2$,⁹ and the $H+D_2$ ¹⁰ reactions also show that quasiclassical trajectory methods are generally reliable for describing atom–molecule collisions at high energies.

On the other hand, computational challenges of obtaining QM reactive cross sections remain formidable for a very large number of reactions of chemical interest. In the case of the two reactions mentioned in the title, namely, $O+HCl$ and the reverse reaction, $Cl+OH$, reaction probabilities for non-zero $J \geq 100$ are required in order to get well-converged QM cross sections. Such calculations are very time consuming and, in many cases, calculations are practical only for the J

^{a)}Electronic mail: ramu@chem.latech.edu

=0 case. Thus far, to the best of our knowledge, QM-QCT comparisons for $J=0$ have been done for only the case where the initial diatomic rotational quantum number $j=0$ (for example, see Ref. 11), the only exception being a recent work by us.¹² In the case $j=0$, trajectories can be forced to have $J=0$ by setting the impact parameter b for all trajectories identically equal to zero. The effect of setting $b=0$ is to force the orbital angular momentum \mathbf{l} to vanish so that $\mathbf{J}=\mathbf{j}_r$. However, to obtain $J=0$ QCT reaction probabilities for initial states with $j>0$, and ultimately to obtain cumulative reaction probabilities, additional restrictions on the initial conditions have to be enforced. This paper describes a way by which this may be accomplished. The prescription for selecting QCT initial conditions is tested by comparing $J=0$ QCT initial state-resolved as well as cumulative reaction probabilities with analogous QM results for the O+HCl and Cl+OH reactions.

In cases where QM calculations for $J>0$ are very time consuming or practically impossible, various approximations have been employed to calculate quantities such as the thermal or state-resolved rate coefficients, which can be compared to experimental results. The most popular among these is the J -shifting method, which typically starts with the cumulative reaction probabilities for the $J=0$ case.¹³ Several recent studies have reported thermal rate coefficients calculated by various versions of the J -shifting method for the O+HCl reaction.^{11,12,14–20} Detailed studies¹⁹ reveal that for initial state-resolved dynamics, the simple J -shift approximation is inadequate and that a proper evaluation of $J>0$ probabilities is very important. Thermal rate coefficients, however, were found to be well estimated within 10%–20% error by the simple J -shift approximation. Given the usefulness of the simple J -shifting approach, it is of some interest to examine the behavior of this method when applied to QCT $J=0$ reaction probabilities. We make an attempt in this direction in this work. The J -shifted QCT thermal rate coefficients are compared to those calculated from the full QCT reaction cross sections¹² which include contributions from all relevant J .

The remainder of this paper is organized as follows. In Sec. II, we present the details of the initial state selection in QCT calculations with $J=0$. In Sec. III, the QCT and QM calculations undertaken for this work are described. The results of the QCT calculations for the O+HCl and Cl+OH reactions are compared to analogous QM calculations in Sec. IV. Here, we also compare the rate coefficients calculated from the $J=0$ QCT probabilities using the J -shifting method to those calculated from the full QCT cross sections. We conclude in Sec. V with a summary of this work.

II. TRAJECTORY INITIAL CONDITIONS

Our intention is to examine the initial conditions necessary to generate trajectories with initial diatomic quantum number $j\geq 0$ and total angular momentum $J=0$. We wish the resulting modifications to be minimal and to preserve, as much as possible, the conventions and the initial state selection methods of the traditional approach, as described in Ref. 2.

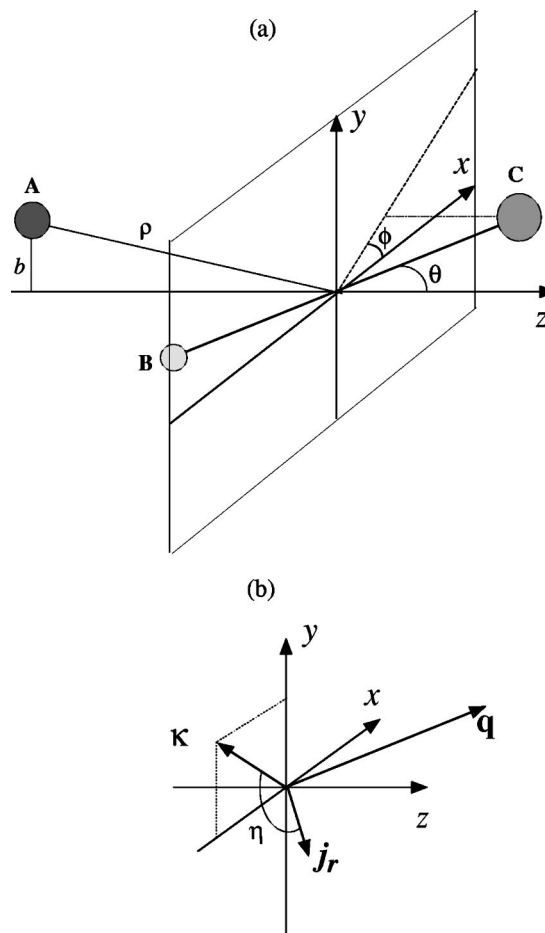


FIG. 1. Traditional (see Ref. 2) definitions of collision parameters used in QCT calculations.

The initial arrangement of the atom A and the diatomic molecule BC commonly adopted in QCT calculations is shown in Fig. 1. The collision parameters b , θ , and η defined in this figure are required for our discussion. The vector \mathbf{q} (with Cartesian components q_1, q_2 , and q_3) points from atom B to C, and the vector \mathbf{Q} (with Cartesian components Q_1, Q_2 , and Q_3) points from the center of mass of BC to the atom A. The convention is to assume that the atom A and the center of mass of BC lie in the yz plane of a Cartesian axes system (i.e., $Q_1=Q_2=0$, where the superscript “0” indicates the initial value) and that the initial relative velocity vector \mathbf{v}_{rel} is directed in the $+z$ direction [i.e., $P_1^0=P_2^0=0; P_3^0=(2\mu_{A,BC}E_{\text{rel}})^{1/2}$]. The total angular momentum of the three atom system, defined as $\mathbf{J}=\mathbf{j}_r+\mathbf{l}$, is obtained by the vector addition of the three components of the rotational and orbital angular momenta. Therefore

$$J^2=\mathbf{J}\cdot\mathbf{J}=J_x^2+J_y^2+J_z^2=(j_x+l_x)^2+(j_y+l_y)^2+(j_z+l_z)^2. \quad (1)$$

With the usual definitions of the Cartesian components of angular momenta, it is possible to show that for the general case we get

$$l_x=b(2\mu_{A,BC}E_{\text{rel}})^{1/2}, \quad l_y=0, \quad l_z=0. \quad (2)$$

Therefore, setting $b=0$ for all trajectories results in the orbital angular momentum being exactly equal to zero, which means $\mathbf{J}=\mathbf{j}_r$. This is, of course, the basis for QCT calcula-

tions for the case $J=j=0$ mentioned earlier. For the more general case $j \geq 0$, it is clear that in order to get $J=0$, the three terms in Eq. (1) must *individually* vanish. We choose to accomplish this without modifying the conventional choices for $\{P_i^0\}$ (given above) and those for $\{q_i^0\}$.² In order for the first term in Eq. (1) to vanish, we require $l_x = Q_2 P_3 - Q_3 P_2 = -j_x$. Since $P_2^0 = 0$, and it is easy to show that, we require

$$Q_2^0 = \frac{-j_x^0}{P_3^0} = \frac{-j_x^0}{(2\mu_{A,BC}E_{rel})^{1/2}}. \quad (3)$$

Similarly, for the second term in Eq. (1) to vanish, we require $l_y = -j_y$. Since $P_1^0 = 0$, this implies that

$$Q_1^0 = \frac{j_y^0}{P_3^0} = \frac{j_y^0}{(2\mu_{A,BC}E_{rel})^{1/2}}. \quad (4)$$

With these definitions, the impact parameter b now depends on the values of j_x and j_y for the particular trajectory and the collision energy. Now, since $l_z = 0$, we require $j_z = 0$. It is easy to show, from Ref. 2, that this requirement translates to

$$j_z = -j_r \sin \theta \cos \eta = 0, \quad (5)$$

where $j_r = |\mathbf{j}_r|$. This condition leaves us with the choice of restricting θ to 0 or π , which restricts the diatomic molecule to be initially oriented along the z axis, or restricting η to $\pi/2$ or $3\pi/2$, which initially restricts the plane of rotation of the molecule, as one might surmise from Fig. 1. Since redefining θ will affect the uniform sampling of $\{q_i^0\}$,² we choose to restrict η , which is randomly assigned to one of the two ‘‘allowed’’ values. These choices, therefore, yield $J=0$ at the beginning of the trajectory propagation. Since the total angular momentum is conserved along a trajectory, the value of J is expected to remain 0 to within the numerical accuracy of the integration procedure.

The collision parameters other than b and η are chosen as described in Ref. 2 by random sampling of appropriate intervals. The restrictions imposed here are comparable to those implicit in the QM $J=0$ case, where \mathbf{l} and \mathbf{j}_r are required to cancel so as to yield $J=0$. Note that with this choice of initial conditions, the total angular momentum J will be identically equal to 0 for all j *regardless* of the way the magnitude j_r is defined.

The definition of j_r is a matter of some interest in QCT calculations. In the quantum-mechanical case, j_r is unambiguously $j_r = [j(j+1)]^{1/2}\hbar$. Some QCT calculations have employed this definition^{4,11} while some others^{6,8-10,21} have opted for the semiclassical expression $j_r = (j + \frac{1}{2})\hbar$,²² which is reported to give better agreement with QM calculations for the $j=0$ case (the difference between the two definitions is insignificant for $j > 0$). In the calculations presented here, we have adopted the semiclassical definition of j_r (and, therefore, of l), but have required that $J \equiv 0$ using the restrictions on η described above.

Arguments can be made that the semiclassical definition should be adopted for the total angular momentum also in QCT calculations, i.e., $|\mathbf{J}| = (J + \frac{1}{2})\hbar$, which would mean that the classical analog of the $J=0$ QM case is $|\mathbf{J}| \equiv \hbar/2$ in QCT calculations. Alternately, in the spirit of the approach taken by Truhlar and co-workers,⁸⁻¹⁰ it can be argued that the total

angular momentum should be allowed to assume any value in the range $0 \leq |\mathbf{J}| \leq \hbar$, because $|\mathbf{J}|$ is the *vector* sum of the rotational angular momentum \mathbf{j}_r and the orbital angular momentum \mathbf{l} , with $|\mathbf{j}_r| = (j + \frac{1}{2})\hbar$, and $|\mathbf{l}| = (l + \frac{1}{2})\hbar$. These choices, of course, have profound implications for the initial conditions. We defer the examination of these issues to the Appendix. Meanwhile, the following argument can be offered to support the choice adopted here, i.e., to set $|\mathbf{J}| \equiv 0$ in spite of the semiclassical definition of $|\mathbf{j}_r|$. The total angular momentum is a rigorously conserved quantity in both QM and QCT calculations. Therefore, although j_r and l can assume arbitrary values in classical calculations regardless of their initial value, the total angular momentum can be given a specific value which is maintained throughout the calculation. In other words, $|\mathbf{J}|$ can be treated as a *quantized* property even in classical calculations. Therefore, it is justifiable to assign the same value to $|\mathbf{J}|$ in both QM and QCT calculations.

III. CALCULATIONS

In this section, we describe the calculations done for the $O(^3P)+HCl$ and $Cl+OH$ reactions, in order to test the method of choosing trajectory initial conditions described in the previous section. The potential energy surface for these calculations is the recently published S4 surface²³ for the lowest $^3A''$ state of the $O(^3P)+HCl$ system, which is based on MRCI+Q/cc-pVTZ energies scaled by the scaled external correlation method.²⁴ Although recent calculations^{12,20} have shown that the S4 surface fails to yield thermal rate coefficients in good agreement with experimental results, especially at low temperatures, it has been shown to reproduce many of the experimental observations^{23,25} of the state-to-state integral cross-section measurements of Zhang *et al.*²⁶

The QCT calculations were done using a modified version of the code used in previous calculations.^{12,23,25} The modifications in the choice of collision parameters are described in the previous section. For the forward reaction, 1000 trajectories were propagated out of each rovibrational state of HCl below the *total* energy of 21 kcal/mol (0.91 eV) with respect to the zero-point energy of the asymptotic $O(^3P)+HCl$ arrangement. This included $v=0$ states up to $j=23$ and $v=1$ states up to $j=16$. For each initial state, batches of trajectories were propagated at collision energies from the maximum value down to the point where the reaction probability was zero (i.e., less than 10^{-3}). The spacing between collision energies was 1.0 kcal/mol or 0.04 eV, except near the reaction threshold where a smaller spacing was used. Also, larger numbers of trajectories (3000–5000) were propagated for collision energies near the reaction threshold so as to decrease the error in the calculated reaction probability. The QCT calculations for the reverse reaction were also done in a similar manner, for OH $v=0, j=0-20$ and $v=1, j=0-15$. In each case, the total angular momentum was monitored and was found to be conserved to within the numerical accuracy of the integration procedure. Typically, we found that the final value of the total angular momentum, $J_f \leq 10^{-31}$. For plotting QCT reaction probabilities as a function of energy, we used a spline interpolant between the re-

action probabilities calculated at the various collision energies.

The QM calculations were done using the method developed by Tolshtikin and Nakamura, using hyperspherical *elliptic* coordinates.^{27,28} The theory and implementation of this method has been described in detail in the cited references and, therefore, we restrict ourselves to a brief outline. The coordinate system consists of the hyper-radius ρ and two angles (ζ, χ) which parametrize the hypersphere. The Schrödinger equation for $J=0$ in these coordinates is written as

$$[K(\rho) + H_{\text{ad}}(\zeta, \chi; \rho) - \mu \rho^2 E] \Psi(\rho, \zeta, \chi) = 0, \quad (6)$$

where $K(\rho)$ represents the kinetic energy for motion in ρ , H_{ad} is the adiabatic Hamiltonian defined at fixed ρ and is composed of the angular kinetic energy and the interaction potential, μ is a characteristic mass factor,²⁷ and E is the total energy. The adiabatic channel potentials $U_\nu(\rho)$ and the channel eigenfunctions $\Phi_\nu(\zeta, \chi; \rho)$ are obtained by solving the eigenvalue problem

$$[H_{\text{ad}}(\zeta, \chi; \rho) - \mu \rho^2 U_\nu(\rho)] \Phi_\nu(\zeta, \chi; \rho) = 0, \quad (7)$$

where ν indicates the adiabatic channel number. After the eigenvalue problem of Eq. (7) is solved at a number of values of the hyper-radius ρ , the radial problem of Eq. (6) is solved by the method of R -matrix propagation. The scattering matrix \mathbf{S} is obtained by imposing the proper scattering boundary conditions on $\Psi(\rho, \zeta, \chi)$ in the asymptotic regions where the entrance and exit channels are fully decoupled. The main advantage of the hyperspherical elliptic formulation is that for the heavy–light–heavy ($H-L-H'$) mass combinations of the type considered here, these coordinates offer good separability between the two hyperangles so that the two-dimensional eigenvalue problem of Eq. (7) can be very efficiently solved at a number of values of the hyper-radius ρ . The hyperspherical elliptic coordinates also make it possible to extend the concept of the potential ridge to three dimensions.²⁸ The potential ridge is defined as the projection of the location (as a function of ρ) of the barrier in the vibrationally adiabatic potentials onto a plot of the $U_\nu(\rho)$. This leads to a view of electronically adiabatic reactions as vibrationally nonadiabatic transitions at avoided crossings in the vicinity of the potential ridge.^{28–31} This approach sheds considerable light on the rather unique behavior of quantum initial state resolved reaction probabilities in this reaction on the S4 surface.¹²

IV. RESULTS AND DISCUSSION

We first compare the QM and QCT cumulative reaction probabilities (CRPs) for the $\text{O} + \text{HCl} \rightarrow \text{OH} + \text{Cl}$, and the $\text{Cl} + \text{OH} \rightarrow \text{HCl} + \text{O}$ reactions. We refer to the former as the “forward” reaction and the latter as the “reverse” reaction. These results are shown in Fig. 2. The origin of the energy axis is the zero-point energy (ZPE) of the asymptotic $\text{O} + \text{HCl}$ arrangement. The solid lines represent the QM probabilities, while the QCT results are represented as dotted lines. The error bars on the QCT cumulative probabilities represent the sum of the error bars for the individual initial state resolved probabilities. It is clear that the QCT and QM results agree quite well with each other, the agreement being

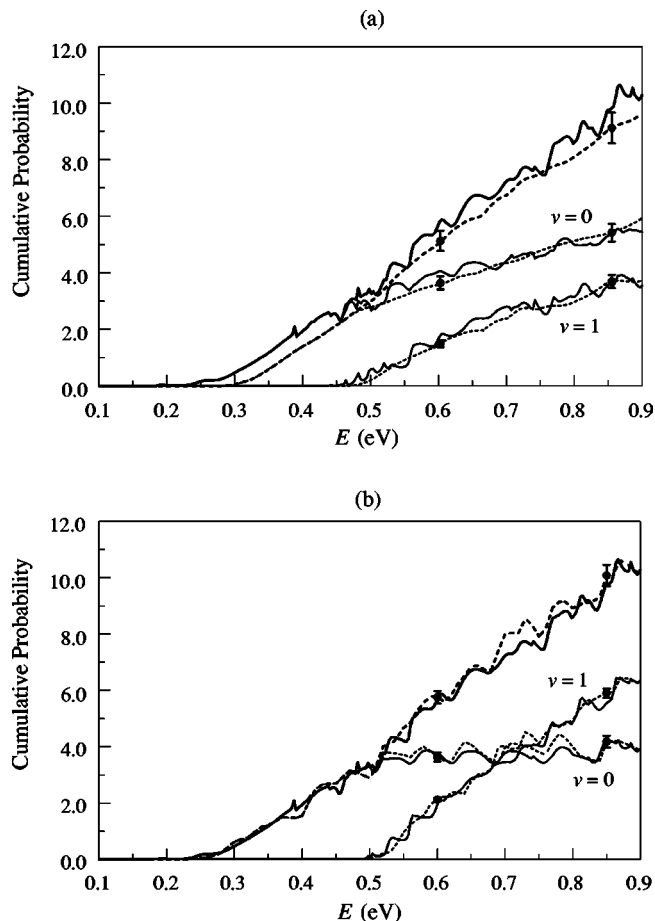


FIG. 2. Comparison of QM and QCT cumulative reaction probabilities for (a) $\text{O}(^3P) + \text{HCl} \rightarrow \text{OH} + \text{Cl}$, and (b) $\text{Cl} + \text{OH} \rightarrow \text{HCl} + \text{O}(^3P)$. The QM probabilities are represented by solid lines and the QCT probabilities, by dotted lines.

especially good for the case of the $\text{Cl} + \text{OH}$ reaction. The vibrationally resolved QM CRPs show qualitatively different behavior in the forward and reverse cases, which is faithfully reflected by the QCT results.

In the case of the QM calculations, the unitarity of the \mathbf{S} matrix (or symmetry of $|\mathbf{S}|^2$) ensures that the CRPs for the forward and the reverse reactions are the same. In QCT calculations, although the principle of microscopic reversibility leads to the expectation that the forward and reverse reactions have nearly the same CRPs, a rigorous constraint does not exist. Therefore, it is not unusual that the QCT results for the reverse reaction are in significantly better agreement with the QM results than for the forward reaction. A possible explanation for this has to do with the extent to which vibrational adiabaticity is conserved in the classical dynamics for the two cases. An examination of the vibrational modes along the minimum energy path (MEP) on the S4 surface indicates that motion along the MEP is only weakly coupled to the vibrational modes transverse to it on the $\text{O} + \text{HCl}$ side of the reaction barrier.³² Therefore, during the approach of the O to the HCl, conditions are favorable for the conservation of vibrational adiabaticity. This means that, in the case of the $\text{O} + \text{HCl}$ reaction, the QCT reaction probability does not assume nonzero values until the total energy approaches that of the *effective reaction barrier*, which consists of the

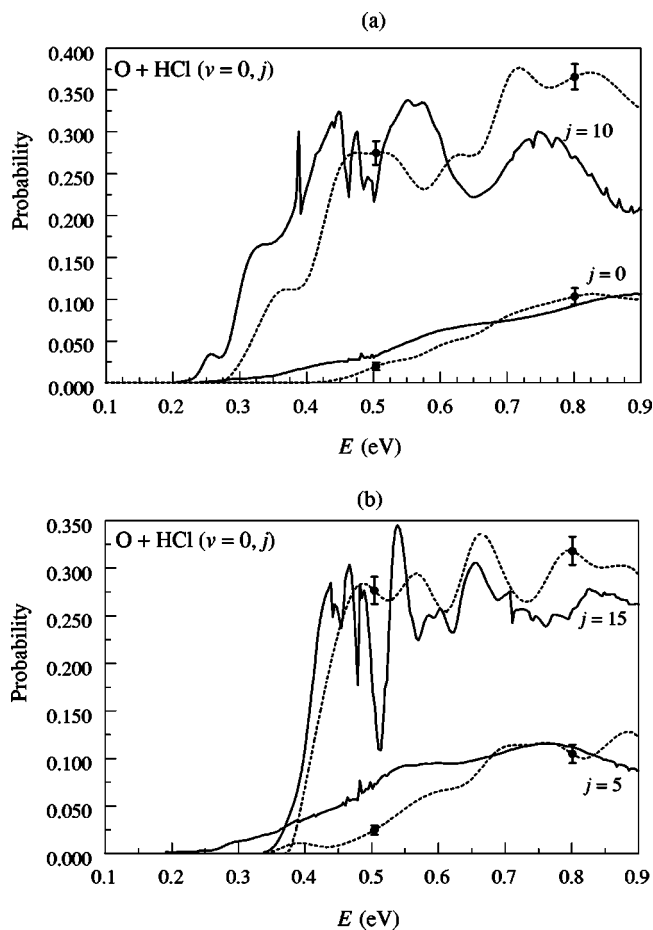


FIG. 3. Comparison of QM and QCT initial state-selected reaction probabilities for the $O+HCl$ reaction. Solid lines represent QM and the dashed lines the QCT results. Panels (a) and (b) compare states with $v=0$ and the indicated initial j values.

Born–Oppenheimer potential barrier, ΔV^\ddagger , plus the local vibrational zero point energy, whereas the QM system tunnels through the effective barrier at lower energies. This behavior is clearly visible in Fig. 2(a). The situation is rather different for the $OH+Cl$ reaction. In this case, a deep (-5.17 kcal/mol with respect to the asymptotic $O+HCl$ energy) van der Waals minimum is present in the entrance channel at $(r_{OH}, r_{HCl}, \theta_{OHCl}) = (1.90a_0, 4.12a_0, 80.4^\circ)$.²³ During the approach of the Cl to the OH, the MEP takes a sharp turn from this minimum to the minimum energy saddle point located at $(r_{OH}, r_{HCl}, \theta_{OHCl}) = (2.42a_0, 2.66a_0, 131.4^\circ)$. All vibrational frequencies associated with the three-atom system undergo significant changes along this rather short distance along the MEP.³² This leads to strong coupling between motion along the reaction path and $O-H-Cl$ vibrational modes, which compromises vibrational adiabaticity. In this case, since classical dynamics does not preserve the zero-point energy, QCT reaction probability assumes nonzero values at $E \approx \Delta V^\ddagger$ which, as seen in Fig. 2(b), leads to very good QCT-QM agreement.

Let us now compare the behavior of QM and QCT reaction probabilities out of a few initial states for the $O+HCl$ reaction. This comparison is presented in Fig. 3, which shows the reaction probabilities out of selected HCl (v

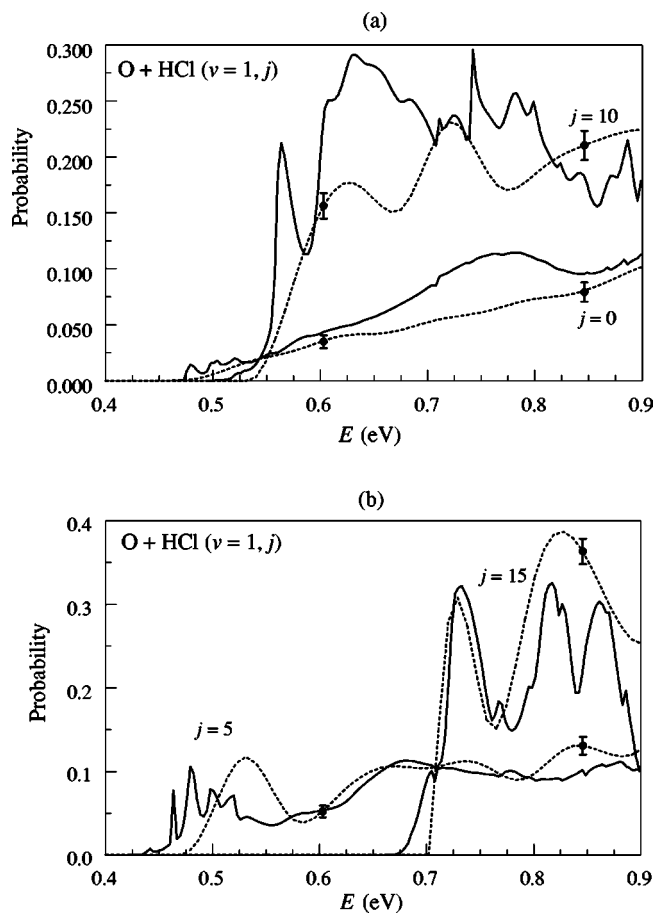


FIG. 4. Same as Fig. 3, but for HCl states with $v=1$ and the indicated j values.

$=0, j$) states and Fig. 4, which shows reaction probabilities for selected HCl ($v=1, j$) states. It is immediately apparent that the QM-QCT agreement is not nearly as good as in the case of the CRPs. However, the energy dependence of the QM and QCT reaction probabilities does exhibit many qualitative similarities while they agree with each other nearly quantitatively in terms of overall magnitudes. Not surprisingly, QCT curves do not show any indications of the sharp resonance structure present in the QM curves, which are indicative of Feshbach resonances.¹² On the other hand, the broader features of the QM curves are reflected to some extent in the QCT results and the degree of this reflection becomes greater as j increases.

The QM and QCT reaction probabilities out of selected initial states for the $Cl+OH$ (v, j) reaction are presented in Figs. 5 and 6. The comments made in relation to Figs. 3 and 4 are applicable here also. The energy dependence of the QCT initial state resolved reaction probabilities show qualitative similarities to their QM counterparts and, once again, the quality of agreement between the two types of results improves as j increases.

There is one aspect of the $OH(v=0, j)$ probabilities that deserves additional comment. In the QM case, it has been observed that reaction probabilities out of the $OH(v=0, j=0-3)$ are surprisingly small over the entire energy range considered,¹² especially when compared to the results ob-

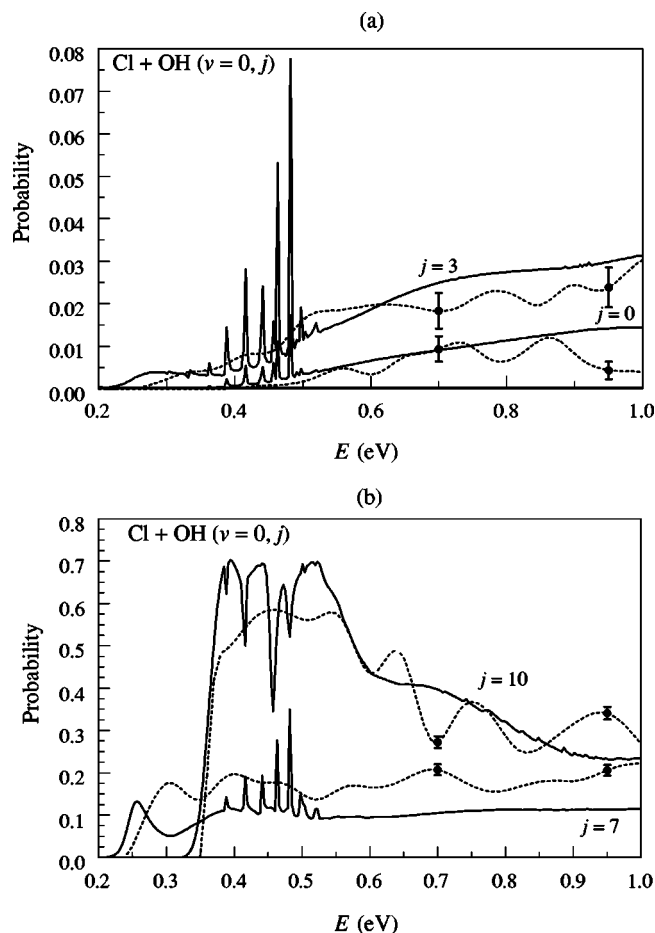


FIG. 5. Comparison of QM and QCT initial state-selected reaction probabilities for the Cl+OH reaction. Solid lines represent QM and the dashed lines the QCT results. Panels (a) and (b) compare states with $v=0$ and the indicated initial j values.

tained on the potential surface of Koizumi, Schatz, and Gordon (KSG).¹⁴ The concept of the potential ridge²⁸ is very helpful in understanding this behavior. Recall that this concept leads to the view of reactive transitions as vibrationally nonadiabatic transitions at avoided crossings in the vicinity of the potential ridge. Avoided crossings elsewhere in the hyper-radial space are far less effective in causing reaction. The main reason for this is the weak interaction between the states correlating asymptotically with reactant and product states away from the potential ridge and the “reaction zone.” The coupling between two states undergoing an avoided crossing is indicated by the magnitude of the energy splitting between them. Sharp avoided crossings with narrow splittings imply weak interaction, while relatively large energy splittings are indicative of substantial interaction between the states. A quantitative judgment about the strength of the interaction between the levels can be made using the parameter a^2 defined in Ref. 33. The adiabatic potential curves for the OH($v=0, j=0-3$) states undergo a few sharp avoided crossings away from the three-body interaction region but, in fact, miss the potential ridge region altogether. We refer the reader to Fig. 4 of Ref. 12 to examine the potential energy curves. The situation is quite different for the $j=7$ and 10 states. The former undergoes multiple sharp

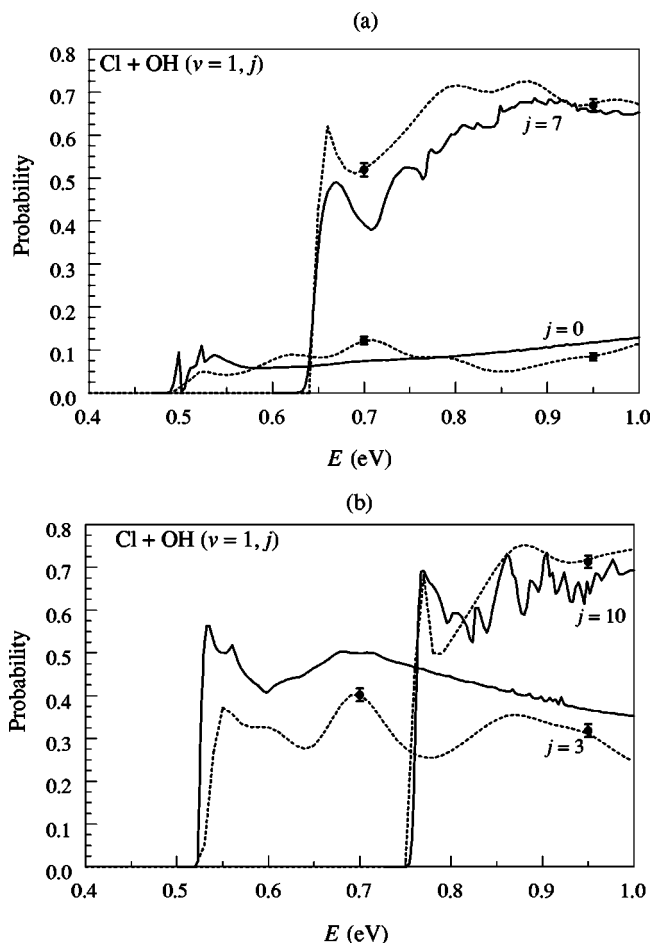


FIG. 6. Same as Fig. 5, but for OH states with $v=1$ and the indicated j values.

avoided crossings in its approach to the potential ridge and appears to undergo a moderately strong (as measured by the energy splitting) avoided crossing with an adiabatic potential curve leading asymptotically to a O+HCl state almost exactly at the potential ridge. The $j=10$ curve undergoes a stronger avoided crossing with an adiabatic potential curve that also leads asymptotically to a O+HCl rovibrational state. In both these cases, we expect the quantum reaction probabilities to be higher and, as can be easily verified from Fig. 5 above, the results bear out these expectations.

The surprising aspect of the comparison in Fig. 5 is that the QCT calculations also lead to similar behavior. The QCT calculations, of course, do not rely on the adiabatic potential curves since these are purely intermediate quantities in a particular approach to the solution of the *quantum-mechanical* reactive scattering problem. However, the relative magnitudes of the QCT reaction probabilities plotted in Fig. 5 show remarkable similarities to the trends observed in the QM case. The QCT probabilities out of OH($v=0, j=0,3$) are extremely small over the entire energy range examined. In sharp contrast, the QCT results for the $j=7$ and 10 states are dramatically larger. This behavior, we believe, indicates that the presence (or absence) of avoided crossings of the adiabatic potential energy curves in the vicinity of the potential ridge is a manifestation of a dynamical mechanism that has

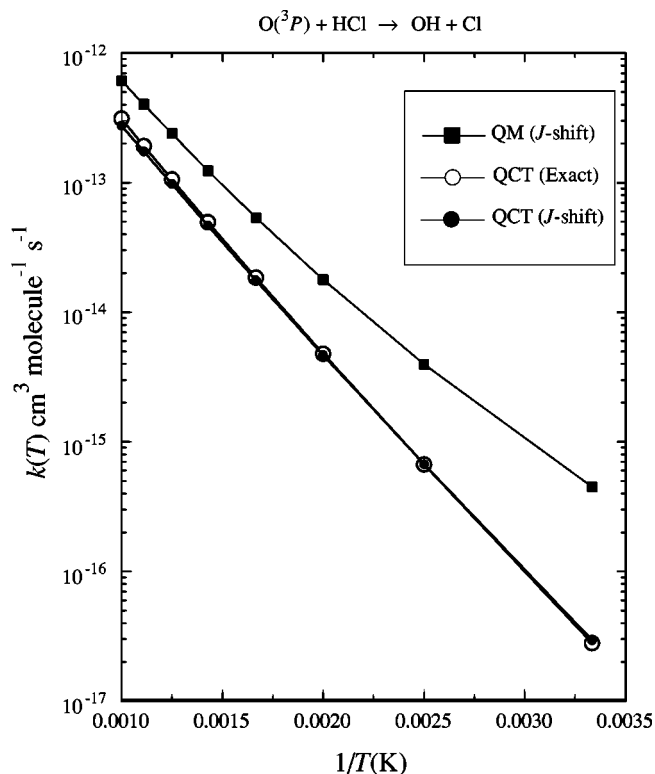


FIG. 7. Comparison of the QM (J -shift), QCT (exact), and QCT (J -shift) thermal rate coefficients.

clear classical analogs. Further insight to this phenomenon is provided by a semiclassical theory of avoided crossings developed by Zhu and Nakamura.³³

Finally, we compare the exact QCT thermal rate coefficients for this reaction¹² to the J -shifted QCT rate coefficients. The reason for making this comparison is the following. As noted in the Introduction, it is generally not straightforward to perform $J > 0$ QM calculations for most reactions of chemical interest. In such cases, the J -shifting approximation provides a simple and reasonably accurate method to calculate the thermal rate coefficients. The basic principle behind the method can be summarized as

$$k_{JS}(T) = k_{J=0}(T) Q_{\text{rot}}^{\ddagger}(T), \quad (8)$$

where $k_{J=0}(T)$ is the rate coefficient calculated from $J=0$ reaction probabilities and $Q_{\text{rot}}^{\ddagger}(T)$ is the rotational partition function for the transition state. Although initial state resolved cross sections and rate coefficients require $J > 0$ dynamics calculations, the simple J -shift approximation is accurate enough for thermal rate coefficients.^{15,18,19} Our recent investigations on the S4 surface¹² have made available the exact QCT thermal rate constants, $k^{\text{QCT}}(T)$, which includes contributions from all relevant values of J , sampled in a statistical manner. The calculations reported above yield the $J=0$ QCT reaction probabilities which permit the $k_{JS}^{\text{QCT}}(T)$ to be calculated at various temperatures. Therefore, we now compare these two quantities with the hope that this comparison will provide some insight into the behavior of the J -shifting method. This comparison is presented in Fig. 7.

It is immediately apparent from Fig. 7 that the exact and approximate QCT rate coefficients are in excellent agree-

ment over the entire temperature range examined. The difference between the QCT and the QM rate coefficients can be attributed to tunneling. Due to the relatively high reaction barrier of the $O+HCl$ reaction, the near-threshold behavior, to which tunneling contributes significantly, has a strong influence on the rate coefficients even at high temperatures. In contrast, the sharp Feshbach resonances which show up prominently in the QM results, but are absent from the QCT ones, are not expected to contribute significantly to the rate coefficients since these get averaged out.

A detailed study of the J -shifting approximation and its variants by Nobusada and Nakamura¹⁹ has shown that the simple J -shifting approximation is not adequate for reproducing quantities such as initial rovibrational state selected cross sections, $\sigma_{vj}(E)$, and rate constants, $k_{vj}(T)$. At least the treatments such as the extended J -shift approximation, which involves QM calculations for $J \leq j_i, J_1, J_2, \dots$, where J_1 etc., represent J values higher than j_i , are required in this regard. However, thanks to the cancellation of over- and underestimates of the individual $k_{vj}(T)$, the simple J -shift approximation seems to work relatively well within 10%–20% for the thermal rate coefficients. From the comparison above, it is seen that the simple J -shifting approximation works exceedingly well in the present system also for QCT rate coefficients.

V. SUMMARY

We have presented a method for choosing trajectory initial conditions in simulations of $A+BC$ reactive collisions which makes it possible to generate trajectories for which the total angular momentum $|\mathbf{J}| \equiv 0$ for all values of the initial diatomic rotational quantum number j . One guiding philosophy in the development of the method was to minimize the changes in the initial state selection methods commonly adopted in “traditional” QCT calculations which sample all possible values of J in a statistical manner. Because of this, the method can be implemented with minimal changes to existing $A+BC$ trajectory codes, most of which incorporate the methods outlined in Ref. 2. These calculations are directly comparable to quantum-mechanical reactive scattering calculations for the special case of $J=0$. Given the computational difficulties in performing accurate QM calculations with $J > 0$ for most reactions of chemical interest, this method provides a way to establish the extent to which classical mechanics can be expected to resemble quantum-mechanical results.

The results of our calculations show that the $|\mathbf{J}| \equiv 0$ QCT approach is generally successful in reproducing the behavior of the QM CRPs both qualitatively and quantitatively. The breakdown of vibrational adiabaticity in the entrance channel, as in the case of the $Cl+OH$ reaction, appears to yield particularly good agreement between QM and QCT cumulative reaction probabilities at low energies. The $|\mathbf{J}| \equiv 0$ QCT dynamics is less successful in reproducing QM initial state resolved reaction probabilities. However, the QCT results agree with the QM ones in many cases qualitatively and in some cases quantitatively. The agreement generally improves as the diatomic rotational state j increases. Naturally, QCT results do not reflect any of the sharp Feshbach reso-

nances which prominently show up in the QM results, especially for the Cl+OH reaction, because these are caused by quasibound states supported by a rather deep well in the potential surface. These resonances, however, tend to get averaged out in the CRP curves and, therefore, do not seriously affect the quantum-classical similarities mentioned above. It is also noteworthy that the relative magnitudes of the QCT initial state resolved probabilities show the same trends as the QM case, as illustrated by the two panels of Fig. 5.

We have also compared the thermal rate coefficients calculated from the QCT $|\mathbf{J}|=0$ reaction probabilities using the J -shifting approximation,¹³ $k_{JS}^{\text{QCT}}(T)$, to the exact QCT rate coefficients, $k^{\text{QCT}}(T)$. This comparison reveals that the two quantities are nearly identical to each other in the temperature range $300 \text{ K} \leq T \leq 1000 \text{ K}$. Similar agreement has also been observed for the exact and J -shifted quantum mechanical thermal rate coefficients.¹⁹

Finally, in the Appendix, we consider alternate definitions of $|\mathbf{J}|$ that can be justified on various grounds. Of these, it is seen that the case ($|\mathbf{J}| = \hbar/2, J_z = 0$), where J_z is the z component of \mathbf{J} , yields results very close to those obtained above, both at the level of initial state resolved probabilities and when summed over the initial states. Other choices lead to poor QM-QCT agreement. Therefore, we believe that the approach taken in this paper is a valid way of obtaining QCT reaction probabilities which can be directly compared to the results of $J=0$ QM calculations.

ACKNOWLEDGMENTS

This research is supported in part by the National Science Foundation, through Grant No. CHE 97-12764 and by a Grant-in-Aid for Scientific Research on Priority Area ‘‘Molecular Physical Chemistry’’ from the Ministry of Education, Science, Culture, and Sports of Japan. B.R. is grateful to Professor Kenneth G. Kay for very helpful discussions.

APPENDIX

We now examine the alternate ways of choosing $|\mathbf{J}|$ in QCT calculations mentioned in Sec. II and their implications for the selection of trajectory initial conditions. It will be necessary in the following to make the distinction between the magnitude of the total angular momentum *vector*, $|\mathbf{J}|$, and the total angular momentum *quantum number*, J .

1. Case A: $|\mathbf{J}| \equiv \hbar/2$

Since semiclassically²² $|\mathbf{J}| = (J + \frac{1}{2})\hbar$, the QCT analog of the QM $J=0$ calculations is the case of $|\mathbf{J}| \equiv \hbar/2$. This choice has profound implications for the selection of QCT initial conditions. In this case, we start by randomly partitioning the value of $|\mathbf{J}|$ (i.e., $\hbar/2$) among the three Cartesian components of \mathbf{J} as

$$J_x^2 = \frac{\beta_x}{\beta_x + \beta_y + \beta_z} \left(\frac{\hbar}{2} \right)^2,$$

and so on, where β_x, β_y , and β_z are three random numbers in the interval (0,1). Now

$$Q_1^0 = \frac{-(J_y - j_y)}{(2\mu_{A,BC}E_{\text{rel}})^{1/2}}, \quad Q_2^0 = \frac{(J_x - j_x)}{(2\mu_{A,BC}E_{\text{rel}})^{1/2}},$$

and, since $l_z = 0$, Eq. (5) can be revised to give

$$j_z = j_r |\sin \theta \cos \eta| = J_z. \quad (\text{A1})$$

In other words, we require

$$|\sin \theta| = \frac{J_z}{j_r |\cos \eta|}. \quad (\text{A2})$$

However, since $|\sin \theta|$ must be bounded between the values (0,1), certain restrictions must be placed on the range of values of $\cos \eta$. We require that $j_r |\cos \eta| \geq J_z$, i.e.,

$$\frac{J_z}{j_r} \leq |\cos \eta| \leq 1. \quad (\text{A3})$$

Therefore, $\cos \eta$ must be chosen in a random fashion between these two limits. If β is a random number in the interval (0,1), then the choice of $|\cos \eta|$ can be written as

$$|\cos \eta| = \frac{J_z}{j_r} + \left(1 - \frac{J_z}{j_r} \right) \beta.$$

With this choice, the angle η calculated can be distributed over the interval $(0, 2\pi)$ by randomly assigning the angle to be equal to η or $(2\pi - \eta)$. Substituting the value of $\cos \eta$ into Eq. (A2) for $\sin \theta$, likewise, yields a value of θ which can be distributed over the interval $(0, \pi)$ by randomly assigning the angle to be equal to θ or $(\pi - \theta)$. Note that we are now choosing the angle θ through Eq. (A2) rather than from a random distribution in the interval $(0, \pi)$.

2. Case B: $|\mathbf{J}| \equiv \hbar/2; J_z \equiv 0$

This case also follows from the semiclassical quantization of angular momentum²² which yields, in addition to the condition $|\mathbf{J}| = (J + \frac{1}{2})\hbar$, the condition that the z component of the total angular momentum, $J_z = M\hbar$. Since $M \leq J$, we require that $M=0$ in addition to the $J=0$ requirement. In other words, semiclassically, the total angular momentum vector has a nonzero length but is confined to the xy plane. The initial conditions for this case can be obtained by first partitioning the value of $|\mathbf{J}|$ (i.e., $\hbar/2$) among J_x and J_y as

$$J_x^2 = \beta_x \left(\frac{\hbar}{2} \right)^2, \quad J_y^2 = (1 - \beta_x) \left(\frac{\hbar}{2} \right)^2.$$

From these relationships, Q_1^0 and Q_2^0 are defined as in case A. Since $J_z = 0$, Eq. (5) is once again used to define the value of η and θ is chosen from a random distribution in the interval $(0, \pi)$.

3. Case C: $0 \leq |\mathbf{J}| \leq \hbar$

As already mentioned in Sec. II, an argument can be made for an even more relaxed selection criterion which would allow J to vary between 0 and \hbar . This can be done as follows. The Cartesian components of J are chosen as

$$J_x^2 = \frac{\beta_x}{\beta_x + \beta_y + \beta_z} J^2,$$

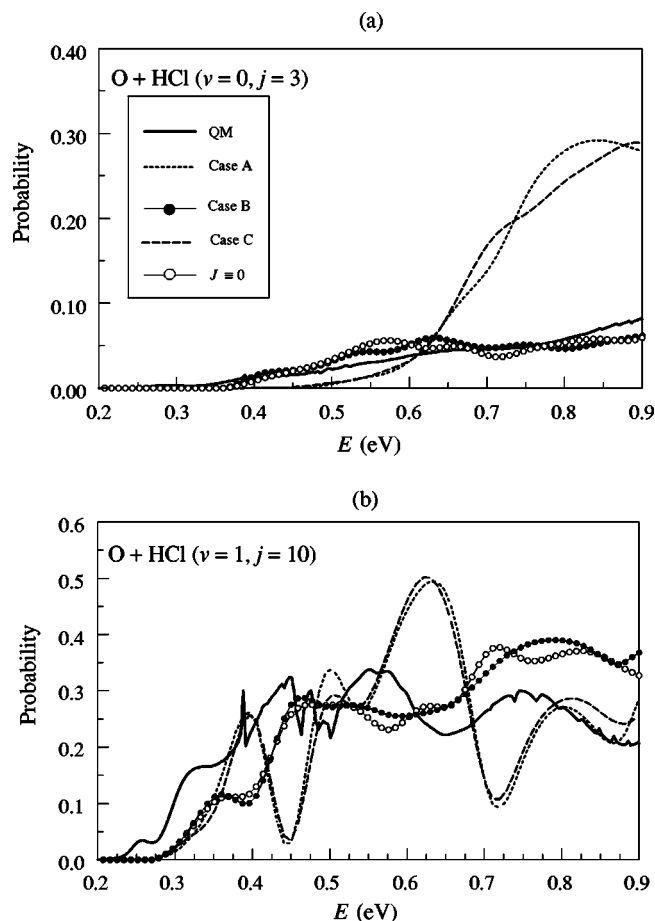


FIG. 8. Comparison QCT reaction probabilities resulting from different choices of $|\mathbf{J}|$ in QCT calculations with QM results. (a) $O+HCl$ ($v=0, j=3$) $\rightarrow OH$ (all)+Cl; (b) $O+HCl$ ($v=0, j=10$) $\rightarrow OH$ (all)+Cl.

and so on, where $|\mathbf{J}|$ is chosen as $\beta\hbar$, where β is a random number in the interval (0,1). Then, steps identical to those for the $|\mathbf{J}|=\hbar/2$ case are employed. This case is clearly in the spirit of the approach taken by Truhlar and co-workers,⁸⁻¹⁰ but has the advantage that since the range of J is strictly limited, no trajectories have to be rejected from the ensemble. Note that this formulation is not applicable to the case where $j=0$ (i.e., $j_r=\hbar/2$). In this case, if the value assigned randomly to $J_z>\hbar/2$, the lower limit of Eq. (A3) will be greater than unity. Therefore, we treat the $j=0$ case by setting $b_{\max}=0$.

We now examine some numerical results from QCT calculations using the two cases presented here and compare them to QM results. For this purpose, classical trajectories were initiated from $O+HCl$ ($v=0, j$) for $j=0,1,3,5,10$, and 15 using the methods for choosing initial conditions described above under cases A, B, and C. In Fig. 8, the reaction probabilities for $j=3$ and 10 thus calculated are compared to QM results and QCT results from the method of choosing initial conditions described in Sec. II, which sets $|\mathbf{J}|\equiv 0$. It is clear that both case A and case C lead to QCT reaction probabilities that are qualitatively quite different from the QM ones for the $j=3$ case, while the curve representing case B is very close to the $|\mathbf{J}|\equiv 0$ case. In the case of $j=10$, all choices lead to poor agreement at low energies. However,

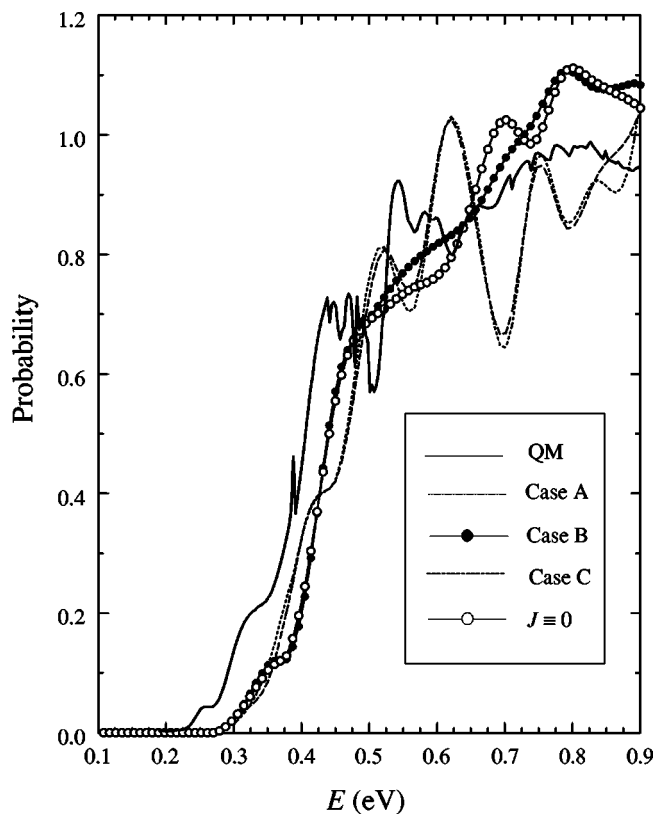


FIG. 9. Comparison, with QM results, of QCT total reaction probabilities out of $O+HCl$ ($v=0, j=0,1,3,5,10,15$) using the three methods of choosing initial conditions discussed in the text.

the curve corresponding to $|\mathbf{J}|\equiv 0$ and to case B are far more similar qualitatively to the QM curve than the other two. Although not shown, we have observed similar behavior in each of the other four states examined. In each case, the results from cases A and C are in good agreement with each other but in poor agreement with the $|\mathbf{J}|\equiv 0$ and case B QCT results and often in qualitative disagreement with the QM results. Also, in each of these cases, the $|\mathbf{J}|\equiv 0$ and case B are quite similar to each other.

We also present, in Fig. 9, a comparison of the partial cumulative reaction probability, i.e., the total reaction probability for states $v=0, j=0,1,3,5,10$ and 15. It is clear from this figure that the specific method employed for choosing initial conditions becomes less important for such “averaged” quantities. However, even at this level, the choice $|\mathbf{J}|\equiv 0$ or ($J=\hbar/2, J_z=0$) appears to give the best qualitative and quantitative agreement with QM results.

¹R. T Pack, J. Chem. Phys. **60**, 633 (1974).

²D. G. Truhlar and J. T. Muckerman, in *Atom-Molecule Collision Theory: A Guide to the Experimentalist*, edited by R. B. Bernstein (Plenum, New York, 1979).

³N. C. Blais, M. Zhao, D. G. Truhlar, D. W. Schwenke, and D. J. Kouri, Chem. Phys. Lett. **166**, 11 (1990); **188**, 368 (1992(E)); D. Neuhauser, R. S. Judson, R. L. Jaffe, M. Baer, and D. J. Kouri, *ibid.* **176**, 546 (1991); W. J. Keogh, A. I. Boothroyd, P. G. Martin, S. L. Mielke, D. G. Truhlar, and D. W. Schwenke, *ibid.* **195**, 144 (1992).

⁴F. J. Aoiz, L. Bañares, M. J. D’Mello, V. J. Herrero, V. Sáez Rábanos, L. Schnieder, and R. E. Wyatt, J. Chem. Phys. **101**, 5781 (1994); L. Schnieder, K. Seekamp-Rahn, J. Borkowski, E. Wrede, K. H. Welge, F. J.

- Aoiz, L. Bañares, M. J. D'Mello, V. Sáez Rábanos, and R. E. Wyatt, *Science* **269**, 207 (1995).
- ⁵E. Rosenman, S. Hochman-Kowal, and M. Baer, *Chem. Phys. Lett.* **239**, 141 (1995).
- ⁶J. F. Castillo, B. Hartke, H.-J. Werner, F. J. Aoiz, L. Bañares, and B. Martínez-Haya, *J. Chem. Phys.* **109**, 7224 (1998).
- ⁷M. Alagia, N. Balucani, L. Cartechini, P. Casvecchia, G. G. Volpi, F. J. Aoiz, L. Bañares, T. C. Allison, S. L. Mielke, and D. G. Truhlar, *Phys. Chem. Chem. Phys.* **2**, 599 (2000).
- ⁸M. Zhao, M. Mladenovic, D. G. Truhlar, D. W. Schwenke, Y. Sun, D. J. Kouri, and N. C. Blais, *J. Am. Chem. Soc.* **111**, 852 (1989).
- ⁹N. C. Blais, M. Zhao, M. Mladenovic, D. G. Truhlar, D. W. Schwenke, Y. Sun, and D. J. Kouri, *J. Chem. Phys.* **91**, 1038 (1989).
- ¹⁰M. Zhao, D. G. Truhlar, N. C. Blais, D. W. Schwenke, and D. J. Kouri, *J. Phys. Chem.* **94**, 6696 (1990).
- ¹¹F. J. Aoiz, L. Bañares, J. F. Castillo, M. Menéndez, and J. E. Verdasco, *Phys. Chem. Chem. Phys.* **1**, 1149 (1999).
- ¹²K. Nobusada, H. Nakamura, Y. Lin, and B. Ramachandran, *J. Chem. Phys.* **113**, 1018 (2000).
- ¹³J. M. Bowman, *Adv. Chem. Phys.* **61**, 115 (1985); Q. Sun, J. Bowman, G. C. Schatz, J. Sharp, and J. N. L. Connor, *J. Chem. Phys.* **92**, 1677 (1990); J. M. Bowman, *J. Phys. Chem.* **95**, 4960 (1991).
- ¹⁴H. Koizumi, G. C. Schatz, and M. S. Gordon, *J. Chem. Phys.* **95**, 6421 (1991).
- ¹⁵W. H. Thompson and W. H. Miller, *J. Chem. Phys.* **106**, 142 (1997); **107**, 2164 (1997).
- ¹⁶B. Poirier, *J. Chem. Phys.* **108**, 5216 (1998).
- ¹⁷K. Moribayashi and H. Nakamura, *J. Phys. Chem.* **99**, 15410 (1995); K. Nobusada, K. Moribayashi, and H. Nakamura, *J. Chem. Soc., Faraday Trans.* **93**, 721 (1997); **94**, 183 (1998).
- ¹⁸M. Matzkies and U. Manthe, *J. Chem. Phys.* **110**, 88 (1999); **112**, 130 (2000).
- ¹⁹K. Nobusada and H. Nakamura, *J. Phys. Chem. A* **103**, 6715 (1999).
- ²⁰S. Skokov, T. Tsuchida, S. Nanbu, J. M. Bowman, and S. K. Gray, *J. Chem. Phys.* **113**, 227 (2000).
- ²¹V. M. Azriel, G. D. Billing, L. Yu. Russin, and M. B. Sevryuk, *Chem. Phys.* **195**, 243 (1995).
- ²²M. S. Child, *Semiclassical Mechanics with Molecular Applications* (Clarendon, Oxford, 1991), p. 78.
- ²³B. Ramachandran, E. A. Schrader III, J. Senekowitsch, and R. E. Wyatt, *J. Chem. Phys.* **111**, 3862 (1999).
- ²⁴F. B. Brown and D. G. Truhlar, *Chem. Phys. Lett.* **117**, 307 (1985).
- ²⁵B. Ramachandran, *J. Chem. Phys.* **112**, 3680 (2000).
- ²⁶R. Zhang, W. J. van der Zande, M. J. Bronikowski, and R. N. Zare, *J. Chem. Phys.* **94**, 2704 (1991).
- ²⁷O. I. Tolstikhin and H. Nakamura, *J. Chem. Phys.* **108**, 8899 (1998).
- ²⁸K. Nobusada, O. I. Tolstikhin, and H. Nakamura, *J. Chem. Phys.* **108**, 8922 (1998).
- ²⁹K. Nobusada, O. I. Tolstikhin, and H. Nakamura, *J. Phys. Chem. A* **102**, 9445 (1998).
- ³⁰K. Nobusada, O. I. Tolstikhin, and H. Nakamura, *J. Mol. Struct.: THEOCHEM* **461–462**, 137 (1999).
- ³¹G. V. Mil'nikov, O. I. Tolstikhin, K. Nobusada, and H. Nakamura, *Phys. Chem. Chem. Phys.* **1**, 1159 (1999).
- ³²S. Skokov, S. Zou, J. M. Bowman, T. C. Allison, D. G. Truhlar, Y. Lin, B. Ramachandran, and B. C. Garrett, *J. Phys. Chem. A* (to be published).
- ³³C. Zhu, H. Nakamura, and K. Nobusada, *Phys. Chem. Chem. Phys.* **2**, 557 (2000).

Journal of Chemical Physics is copyrighted by AIP Publishing LLC (AIP). Reuse of AIP content is subject to the terms at: <http://scitation.aip.org/termsconditions>. For more information, see <http://publishing.aip.org/authors/rights-and-permissions>.